Thermal cycling damage monitoring of thermal barrier coating assisted with LASAT (LAser Shock Adhesion Test)

Vincent Maurel, Vincent Guipont, Mélanie Theveneau, Basile Marchand, Florent Coudon

Version of Record: https://www.sciencedirect.com/science/article/pii/S0257897219310394
Manuscript_c79cc5702b75ba9382b4d14e72803ee6

Thermal cycling damage monitoring of thermal barrier coating assisted with LASAT (LAser Shock Adhesion Test)

Vincent Maurel[a,*], Vincent Guipont[a], Mélanie Theveneau[a], Basile Marchand[a], Florent Coudon[b]

[a] *MINES ParisTech, PSL University, MAT - Centre des Materiaux, CNRS UMR 7633, BP87, 91003 Evry, France*
[b] *Materials and Processes department, Safran Tech, Safran SA, Rue des Jeunes Bois, Châteaufort 78772 Magny-Les-Hameaux*

Abstract

One of the major challenges for thermal barrier coating (TBC) system is to determine the time to failure of ceramic layer during aging. The aim of this paper is to propose new methodologies for experimental assessment of adhesion and for analysing its link to lifetime to spallation. Recently, the use of LAser Shock Adhesion Test (LASAT) with multi-shock experiments have shown its capability for both ranking different coating solutions in terms of adhesion and evaluating its evolution with aging. The methodology developed in this study is based on single shock experiments using the same laser parameters in order to measure non destructively and compare directly the resulting crack sizes and corresponding interface strength levels during interrupted thermal cycling. This cycle-by-cycle non destructive methodology was also enriched by the assessment of the evolution of the interfacial damages that were first initiated by LASAT and further propagated during subsequent thermal cycling. The evolution of interfacial damages during thermal cycling was shown to be consistent with interfacial delamination measured post-mortem by cross-sectioning. Besides, the influence of dwell time at high temperature has been clearly established, confirming that short dwell time was more detrimental as compared to longer and conventional dwell used for thermal cycling tests at high temperature.

Keywords: thermal barrier coating, interface strength, adhesion, LASAT, thermal cycling frequency

1. Introduction

Thermal Barrier Coatings (TBC) are widely used to protect the warmest components of aeroengine turbines. Two main objectives are pursued to design such coatings which are (i) a low thermal conductivity in order to reduce the temperature at the surface of the

*Corresponding author
Email address: vincent.maurel@mines-paristech.fr (Florent Coudon)

substrate and (ii) a resistance to several environmental degradation mechanisms such as oxidation, corrosion and attack from external products (e.g. calcium-magnesium-alumino-silicate (CMAS) [1, 2]). One widespread TBC solution is composed of a ceramic layer, the so-called Top Coat (TC) and a metallic bond-coat (BC) which respectively act on the thermal flux and on passivation effect forming a reservoir for thermal grown oxide (TGO). The TC could be made of partially stabilized yttria (YSZ) processed either by electron beam physical vapor deposition (EB-PVD) or by air plasma spray (APS) [3, 4]. The BC being made of Al- or Cr-rich metal deposited mostly by diffusion process or overlay coating. The success of these solutions is based on an improvement of the life of the complete TBC system, including the chosen substrate material, for typical creep, fatigue or thermo-mechanical fatigue loading. Despite the increasing demand on technology improvement of coating, making solution precursor plasma spray (SPPS or SPS) TC deposition process as promising solutions [5, 6], few robust models predicting the life of TC to spallation are available for TBCs.

Among them, pioneer works of Miller et al [7, 8] have established that TGO thickening and strain arising from coefficient of thermal expansion (CTE) mismatch between TBC layers during thermal cycling drive damage evolution. Such approach was improved considering damage induced by oxide growth and damage induced by thermal cycling and subsequent straining respectively [9]. Alternative model have promoted the modeling of the out-of-plane stress based on a local analysis of interfacial undulation and its evolution with rumpling. Analyses was done either by means of full-field simulations at the micron scale [10, 11, 12] or using analytical models derived from the von Karman theory for the nonlinear deformation of curved plate [13, 14]. In order to identify the parameters of the chosen model, different approaches have been proposed to evaluate interfacial damage. Compressive testing after aging yields an inverse analysis method to derive a damage evolution [15]. Another proposition is to associate the reduction of interfacial toughness computed through an energy analysis of bending experiments to an interfacial damage evolution [16, 17]. Numerous experiments have been carried out to track coupling between aging and interfacial toughness for different number of cycles, maximum temperature, dwell time at high temperature and shear modes [18, 9, 19, 17]. But all of these destructive approaches make quantifying the evolution of mechanical properties time-consuming because of the large amount of specimen to analyze. Otherwise, the large scatter of TBC performance in the as-processed condition [20] are embedded in measurements and could lead to some wrong conclusions.

Recent works achieved on typical APS-MCrAlY system have been based on fatigue crack growth analysis [21]. Such an approach appears to be fully relevant for thermo-mechanical fatigue (TMF) loading experienced in-service for coated components. For disks coupons under thermal cycling, APS TC debonding is a continuous process [3] whereas for EB-PVD TC, most of observed spallation are unstable and/or driven by edge effects [22]. This point limits the use of fatigue analysis to assess damage of EB-PVD TBC.

Recently, the use of laser shock to promote interfacial debonding and measure adhesion has appeared as a very interesting tool for various coating systems. Its principle is to use laser-to-matter interaction to induce a compressive shock wave in the coated system. After reflexion on the free surface, this shock-wave becomes tensile and can promote

the coating/substrate debonding, if the tensile stress level is high enough and if the coating/substrate interface is the weak point of the system (see Fig. 1). A large amount of work has been achieved to determine the range of applicability of LAser Shock Adhesion Test, and has been successful for plasma spray or EB-PVD YSZ coatings for high temperature application but also for hydroxyapatite for bio-coating solutions [23]. A multi-shock methodology involving a range of laser power density has enabled to establish the so-called LASAT-2D curves to test adhesion. These LASAT-2D curves are characterized by the definition of the evolution of the size of the debonded area as a function of the laser power density involving two-dimensional effects on shock-wave propagation. Besides, for each coated system, the minimum energy below which neither interfacial delamination nor interfacial damage is observed corresponds to the so-called LASAT threshold (state I in Figure 1). Therefore, by selecting a quality criterion associated to a given condition of laser shock, single-shock LASAT can also be envisaged in order to control non destructively the integrity of a coating during its life [24]. In the case of EB-PVD YSZ, it has been also established that LASAT

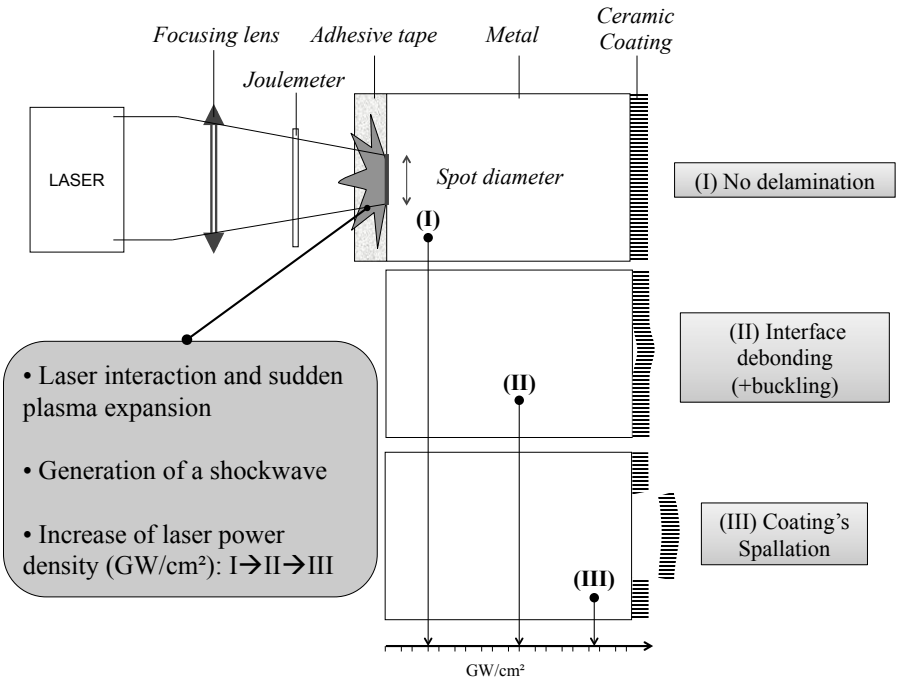

Figure 1: LASAT principle

was straightforward to rank different process conditions consistently with life to spallation for thermal cycling aging [25, 26]. Even though some of the mechanisms leading to interfacial debonding by laser shock remain unclear, it has also been observed that the debonded interface by LASAT for thermally cycled specimens was the TC/TGO interface [26]. In the case of EB-PVD YSZ with (Ni,Pt)Al BC, it has been widely observed that thermal cycling induces damage at the TC/TGO interface leading to interfacial cracking and final spallation of the TC [27, 22, 3, 9, 28, 19]. Then, authors in [25, 24, 26] have combined LASAT with

thermal cycling and shown that the debonded area induced by the laser shock increases with aging: an initial decohesion evolves under further thermal cycling firstly by increasing the height of the associated blister and secondly by increasing the debonded area at a certain amount of thermal cycles. Besides, authors have also proposed to carefully determine interfacial toughness at the point of further debonding [26]. However this study was limited to few samples and a unique thermal cycling condition. So that LASAT-2D curves seem to be sensitive to interfacial damage. This point is particularly important to validate LASAT for TBC design optimization. LASAT has appeared to be a very promising tool for interfacial toughness assessment because of its exceptionally low experimental scatter induced by the test itself as compared to other testing methods. For the time being, a proof of concept is needed to push its application in realistic conditions involving both the variation of thermal cycling parameters and the discrepancy of each TBC sample submitted to LASAT experiments.

The aim of the present study is the development of a robust experimental methodology based on LASAT to characterize interfacial damage evolution varying thermal cycling testing conditions for a large batch of TBC coupons.

2. Materials, specimens and experimental methodology

2.1. Materials and specimens

The studied TBC system is made of AM1, a first generation Ni base single crystal superalloy (SX), using a (Ni,Pt)Al bond-coat, processed by Aluminizing (aluminizing phase vapor snecma APVS) and an EB-PVD 7YSZ ceramic top-coat. Specimens are made of disk coupons of 25 mm in diameter and 1 mm in thickness. The disks were machined from a single round bar of Ni-base SX, the plane side of the disk being orthogonal to the [001] direction of the bar. APVS for BC and EB-PVD for TC have been achieved in a single batch for a series of 28 specimens. In the as-processed condition, the external BC thickness is about 50 μm, the TGO thickness is about 0.5 μm and the TC is about 150 $\pm$ 5μm. Before thermal cycling, the coated disks have been chamfered using P400 SiC paper.

2.2. Thermal cycling

Thermal cycling has been achieved in two distinct conditions. The first one is a conventional isothermal furnace (Delta Thermique, France) using a 10-50-15 minutes cycles for heating, high temperature (HT) dwell and cooling respectively, and will refer to the long dwell furnace cycle test (L-FCT) in the sequel. A plate which can host a series of 24 specimens, moves from air lab to the furnace and back in the air lab. For each cycle and at the end of the cooling step, a photograph of the set of specimens is made to monitor macroscopic spallation if any. In addition, the test is interrupted every hundred cycles to inspect carefully each specimen.

The second thermal cycling carried out is an in-house set-up consisting in a smaller furnace, where only 6 specimens can be tested in a single run. The associated cycle consists in 5-5-5-5 minutes for heating, HT dwell, cooling and low temperature dwell respectively, and will refer to the short dwell furnace cycle test (S-FCT) in the sequel. For both tested

conditions, the minimum temperature was set to 100 °C and the dwell temperature to 1100 °C. The temperature was controlled with thermocouples, one located on the support used to hold the specimens and the other 5 mm above the support.

For the L-FCT, 15 specimens and for the S-FCT, 6 specimens have been cycled respectively. In addition to that, 7 samples have been used to establish LASAT-2D curves detailed in the sequel.

2.3. Observation methods

Visual inspection was systematically achieved after each interruption in order to assess the macroscopic spallation just after laser shock or induced by thermal cycling. The interfacial delamination was thoroughly analyzed by means of light microscope and infra-red inspections. Using optical imaging, the intensity of reflected light is enhanced by the presence of an air gap between the metal and the TC leading to a contrast between the debonded area and the rest of the coating in top-view observation. Visual inspection or image analyses based on grey-level thresholding can be achieved. Therefore, the limit of the debonded area can be obtained by implementing the so-called "white-spot" diagnostic, see figure 2(b). However, for small size debonded areas, this diagnostic might be limited. Therefore, infrared thermography was also systematically combined to optical imaging.

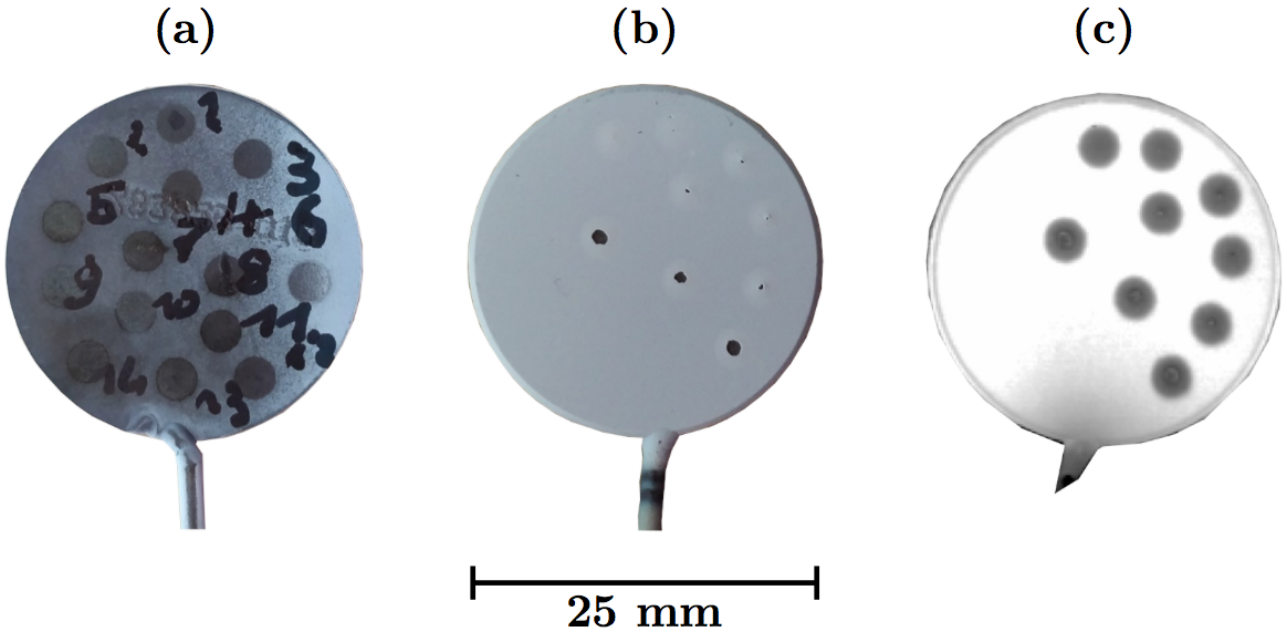

Figure 2: After laser shock achieved for LASAT-2D curve (a) substrate side (b) coating side optical imaging (c) coating side infra-red thermography.

Infrared thermography is also known to be sensitive to interfacial debonding for heated specimen [29]. In this case, the presence of the air gap acts as a diffusion barrier for heat that

affects the surface temperature straight to the position of the debonded area. The infrared diagnostic set-up consists in using a heating plate at 50 °C in contact with the substrate side of the specimen. An infrared camera (Titanium serie, Cedip Infrared Systems, France) with a 320x256 pixels sensor in the wavelength range of 1.9-5.1 μm is used to obtain the surface temperature mapping. The infrared sensor and focusing distance led to a spatial digital resolution of 160 μm/pixel. In this work, the quantitative analysis was achieved systematically on infrared images by thresholding to measure the debonded area, see figure 2(c). For sake of simplicity, the measured area of debonding was associated to an equivalent disk on which the diameter is referred as the debonded diameter in the sequel. It has been shown on plasma sprayed alumina coating that the systematic error induced by the infrared method was less than 100 μm, by comparing the measured diameter from white-spot diagnostic and cross-sectioning [30]. This yields to a systematic error of less than 10% over the measurement of the debonded diameter which minimum value is of about 1 mm.

2.4. LASAT facility and experiments

LASAT experiments are achieved using a Nd-YAG laser source (SAGA 330, Thales, France) at 532 nm with a top-hat energy distribution and a 5.2 ns pulse duration. The laser irradiated area is selected by a converging lens while the laser energy can vary from 0.1 to 2.0 J using a polarizer. A transparent adhesive tape stuck on the metallic side as confinement medium was preferred in order to prevent water to be in contact with TBCs. LASAT is implemented by selecting different laser power densities (0.02 to 8 GW.cm^{-2} typically) to evaluate the debonding behaviour (see the figure 1). For each sample and for a fixed laser diameter, multi-shock experiments were done by implementing a series of laser shock with increasing laser energy. Such experiment allow to draw LASAT-2D curve by plotting the debonded areas measured by infrared imaging in function of the increasing laser power density (same laser diameter). In case of single shock experiments, both laser diameter and laser energy were kept constant. Thus, laser shock and corresponding infrared imaging could be repeated on different location of the same coated sample after each interrupted thermal cycle to investigate the stability or the evolution of the crack size and assess the corresponding evolution of the interface strength according to the LASAT approach.

2.4.1. LASAT-2D curves

The adhesion level was evaluated by establishing LASAT-2D curves on TBC disk samples in the as-processed state and after 113 L-FCT cycles. The laser shock diameter was set to 3.1 mm and applied laser power density ranges from 0.2 to 3.0 GW.cm^{-2} involving a maximum of 13 different locations for the shocked areas, see Figure 2(a). All specimens have been measured using both optical and infrared methods detailed in section 2.3.

2.4.2. Single laser shock

Single laser shock experiments have been first achieved in the as-processed condition for each sample. The laser shock was set to 3.1 mm and laser power density selected at 1.18 GW.cm^{-2} based on a previous LASAT campaign [24]. This LASAT condition was chosen to insure both the occurrence of debonding, and besides that the debonded area is

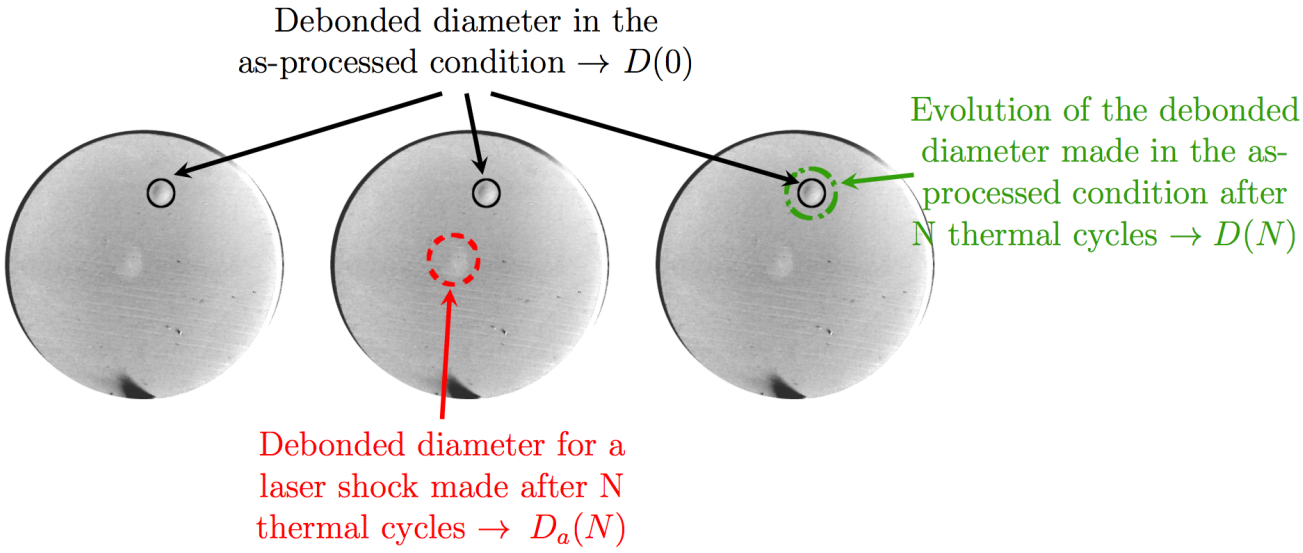

Figure 3: The two kinds of damage monitoring investigated during thermal fatigue aging by means of the laser shock technique

large enough to obtain a good ratio between spatial resolution of infrared measurement and actual size of the debonded area. After interruption of L-FCT or S-FCT, TBC samples have been shocked again using the same laser condition on another position. If no drastic macroscopic spallation occured, the thermal cycling test could continue until a second interrupted number of cycles. All tested conditions combining single laser shock experiments and thermal cycling are given in Table 1 summarizing the first number of cycle (N_1) and the second number of cycle (N_2) where LASAT has been achieved for each TBC sample submitted to L- or S-FCT. Most samples has experienced shocks in as-processed condition, after N_1 and N_2 cycles, leading to 3 shocks for each sample. Debonded areas for the whole batch of specimen have been measured using the infra-red set-up detailed in section 2.3. All data addressed in the sequel considering single shock correspond to debonding with neither observation of TC cracking nor TC spallation.

3. Damage monitoring

3.1. Range of properties in the as-processed and after thermal cycling conditions

In the as-processed condition, the chosen laser power density for single shock experiment was leading to a variation less than 4%. However, a large scatter in the measured diameter of debonded area on each TBC sample in the as-processed condition was observed, see Table 2. Indeed, the debonded diameters were ranging from 1.2 to 3 mm with no correlation with the slight variation of laser power density or with the actual variation in total substrate-coating thicknesses that were ranging from 1.14 to 1.17 mm for this batch of specimens (see Table 2).

Table 1: Specimen number, group specified by initial debonding - see paragraph 3.1 and Table 2 for details, S(hort) or L(ong) dwell time at high temperature for FCT, number of cycles where single laser shock has been achieved for "single shock experiment" - see paragraph 3.2 - and maximum number of thermal cycles. (*) corresponds to specimens used for LASAT-2D curves.

Sample #	group	FCT	N_1	N_2
24	1	-	-	(*)
02	2	-	-	(*)
10	2	-	-	(*)
27	3	-	-	(*)
25	1	L	-	113 (*)
28	2	L	-	113 (*)
30	3	L	-	113 (*)
04	1	L	100	589
06	2	L	100	589
11	3	L	100	589
13	1	L	206	695
12	2	L	206	695
14	3	L	206	695
15	1	L	287	603
16	1	L	287	603
17	2	L	287	603
18	1	L	400	606
19	2	L	400	606
20	3	L	-	400
22	3	L	400	606
21	2	L	507	585
23	1	L	507	585
31	2	S	-	892
32	2	S	-	2000
33	3	S	-	892
36	3	S	-	892
34	3	S	-	1607
35	3	S	-	2000

Because no bias in measurement was evidenced, the observed scatter is assumed to reflect a significant variety of interface strength from sample to sample in the as-processed condition. Therefore, we decided to assign the interfacial strength level exhibited in the as-processed condition into three groups of equivalent number of specimens corresponding to low, medium and high range of debonded area. The stronger interface corresponding to group #1 and the less adherent corresponding to group #3, see associated values for both debonded diameter and total thickness in Table 2. Because, for class #2 the variation of thickness reaches the minimum and maximum measured values of thickness, it confirms that no correlation between observed scatter in debonding and thickness could be assumed.

Table 2: Analysis of the specimens in the as-received condition and group repartition

Group #	Number of specimens	Debonded diameter (mm) (mean value ± std)	Thickness (mm) (mean value ± std)
All specimens	22	2.1 ± 0.47	1.164 ± 0.014
1	7	1.5 ± 0.15	1.172 ± 0.005
2	7	2.1 ± 0.14	1.165 ± 0.017
3	8	2.7 ± 0.13	1.156 ± 0.016

LASAT-2D curves have been achieved in the as-processed condition from 0.2 to 2.7 GW.cm^{-2}. This range of laser power density is covered by one sample of each group, except for group #2 where two samples have been used in order to have a better statistic for this group. The resulting LASAT-2D curves are mostly continuous for each group. Only a slight difference in LASAT-2D position was evidenced between groups #2 and #3 while a significant difference was confirmed when groups #2 and #3 are compared to group #1. Thus, the obtained ranking is consistent with previous observations from single shock experiment: the highest (resp. the lowest) adhesion for single shock leads to the lowest (resp. the highest) diameter of debonded area for the whole range of laser power density (see the Figure 4(a)).

LASAT-2D curves have been also established for one specimen of each groups after 113 cycles of L-FCT in order to investigate the influence of thermal cycling with a multi-shock experiment. The resulting LASAT-2D curves are given in the Figure 4(b). It is obvious that the LASAT-2D curves do not exhibit so much scatter from one group to another as compared to the as-processed condition. Nevertheless, the observed ranking of LASAT-2D curves after this aging time remains consistent but only with a slight difference between groups if compared to the as-processed condition. In the range of laser power density investigated for the LASAT-2D curves, the debonded diameters slightly increase with thermal cycling aging (N=113), except for the group #1 where this trend is more pronounced. Besides, spallation occurs for lower laser power density after aging than observed in the as-processed condition.

3.2. Single shock experiments at different number of cycles

During each selected interruption of L-FCT and S-FCT thermal cycling, a new laser shock has been applied to one specimen of each group with the fixed LASAT parameters

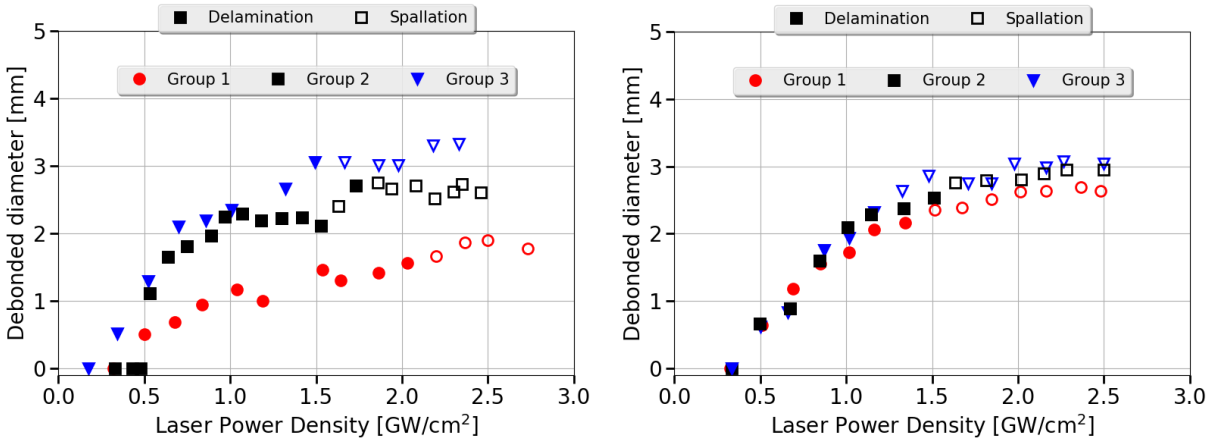

(a) In the as-processed condition

(b) After 113 thermal cycles with the L-FCT condition

Figure 4: LASAT-2D curves (diameter of the debonded area as a function of the laser power density).

(see paragraph 2.4.2 and Table 1 for details). This analysis has been established on 21 specimens. This results in the evolution of debonded diameter as a function of aging for both L-FCT and S-FCT, Figure 5. Considering the whole set of specimens as a function of the number of cycles for L-FCT, it is observed that the scatter observed up to 200 cycles is lower than the scatter in the as-processed condition, Fig. 5(a). In the range 200 to 400 cycles, debonding seems to increase and seems to decrease after 400 cycles. But beyond, 200 cycles the scatter increases and the observed trends in evolution of debonded diameter are not obvious: no clear increase or decrease appears as a function of aging considering the whole set of specimens or considering each group.

To further analyze this effect, the incremental increase of length can be derived from initial diameter of debonding, $D(0)$, and current debonded diameter, $D_a(N)$, using relative incremental increase of debonding $\frac{D_a(N)-D(0)}{D(0)}$. Considering each specimen individually by connecting measured debonded diameter does not clarify the trends of impact of aging in debonding, Fig. 5(b). The impact of dwell time at high temperature is also not evidenced by this analysis.

Because it has been established that the cumulated time drives both oxidation and subsequent damage for the tested system, it could be straightforward to compare any duration of dwell during thermal cycling using the cumulated time spent at maximum temperature $t_{HT} = N.\tau$, where N corresponds to the number of cycles and τ is the duration of the dwell time at the maximum temperature [9]. The observed trends in evolution of increment of debonded diameter are again not obvious, no clear increase or decrease appears as a function of aging, Fig. 5(c). The observed scatter in debonded diameter prevent from interpreting the effect of dwell duration, for evolution of debonded diameter plot as a function of either N or t_{HT}, see Fig. 5(b) or 5(c) respectively.

This scatter could be induced by the group observed in the as-received condition, but no

clear interpretation have been obtained isolating points from each group.

3.3. Interfacial crack evolution with thermal cycling

Another monitoring investigated in this study consists in measuring the evolution of the debonding associated to the laser shock achieved in the as-processed condition being further thermally cycled; the measurement being achieved along the interruptions of thermal cycling, Figure 6. This method exhibits a clear increase in the debonded diameter as a function of the number of cycles for L-FCT for the whole set of specimens as well as for each group, Fig. 6(a).

To further analyze this effect, the relative incremental increase of debonding $\frac{D_a(N)-D(0)}{D(0)}$ has been plot for each specimen as a function of N for both S- and L-FCT, Fig. 6(b). Accounting for the initial scatter, a significant correlation is observed between interfacial cracking and aging: the debonding process appears to be a monotonic function of the number of cycles for both S-FCT and L-FCT, Figure 6(b). At last but not least, S-FCT appears to be more damaging than L-FCT when plot as a function of t_{HT}, Figure 6(c), making obvious the strong impact of cycling as compared to oxidation driven damage mechanism [22, 9].

Cross-section of propagation from a laser shock achieved in the as-processed condition and experiencing L-FCT aging is shown in Figure 7. First, large amplitude of buckling is observed without any observed damage within the TC layer, Fig. 7(a). Magnifications of interface beyond the crack-tip, Fig. 7(b), or at the vicinity of the crack-tip, Fig. 7(d), show that the "natural" damage induced by the thermal cycling aging and the progressive cracking from the initial blister are both localized at the TGO/TC interface. Besides, the blister appears not to modify significantly the interfacial damage. On the other hand, when considering area far from the crack-tip, large rumpling is observed, Fig. 7(c). These observations are consistent with observed debonding from an initial laser shock in [25, 26].

4. Discussion

4.1. Synthesis of results: LASAT and thermal cycling combined

Based on a single laser shock in the as-received condition, the proposition made of ranking the samples by group of initial adhesion has appeared to be consistent with observed adhesion evolution with thermal cycling aging using LASAT-2D curves, Fig 4. But single laser shocks, when shocks are repeated after thermal cycling, have led to a very large scatter as compared to initial range of debonding for a given group of adhesion, Fig. 5. A close view to LASAT-2D curves could explain this point: the target value of 1.18 GW.cm^{-2} is in the as-received condition straightforward to the whole set of samples as it does not produce any TC spallation, see Figure 4(a). However, after thermal cycling, it has been widely commented that the interfacial toughness decreased [31, 22, 16, 9]. Thus, the applied laser shock could lead to some instability for advanced interfacial aging, inducing local cracking and subsequently the observed scatter in debonding. Such a scatter was already evidenced using 4-point bending test [17]. Moreover, the chosen level of laser power density is likely to be too high to avoid complex laser to interfacial damage interactions. When large interfacial damage occurs, it is possible that the shock wave propagation is strongly modified

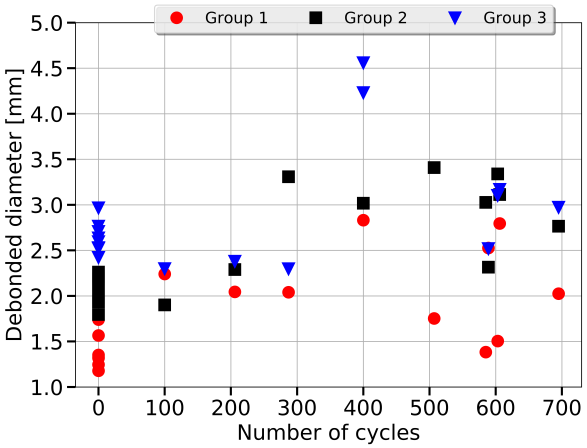

(a) L-FCT function of N

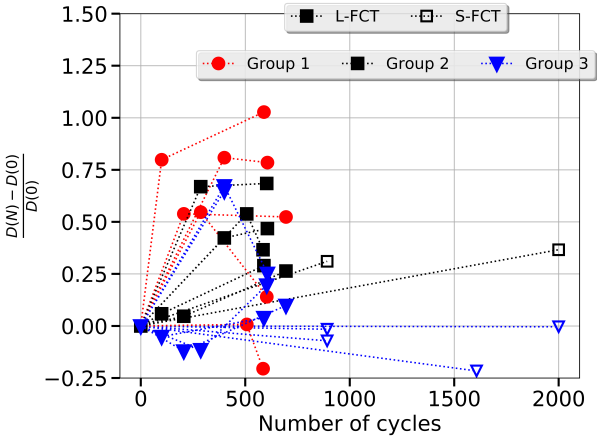

(b) S- and L-FCT function of N

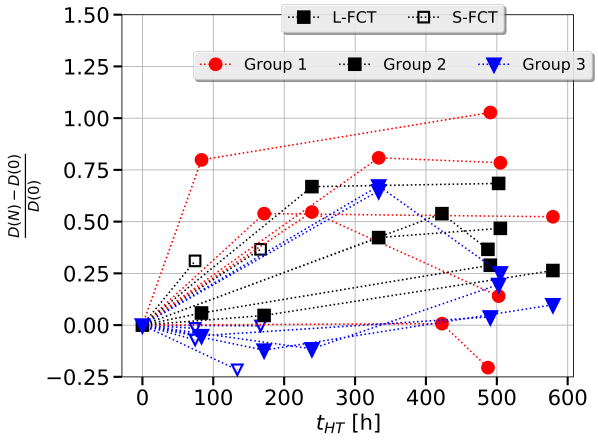

(c) S- and L-FCT function of t_{HT}

Figure 5: Delamination from laser shock achieved at different number of cycles. (a) corresponds to a global group analysis for L-FCT condition and in (b) and (c) dashed lines connect measurement achieved for each specimen at different number of cycles corresponding to Table 1 for both S- and L-FCT

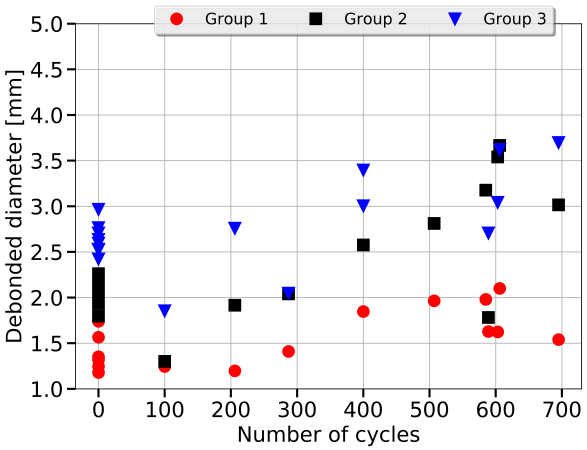

(a) L-FCT function of N

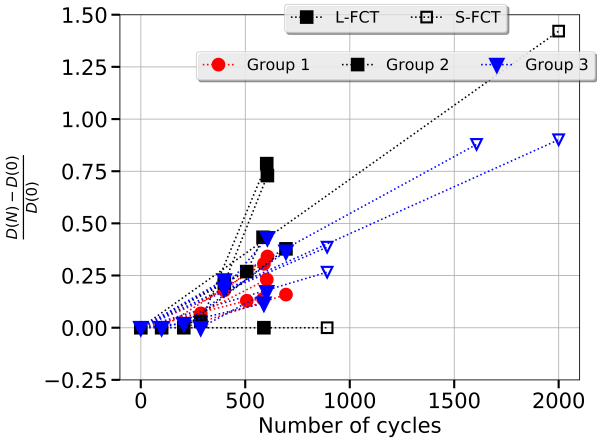

(b) S- and L-FCT function of N

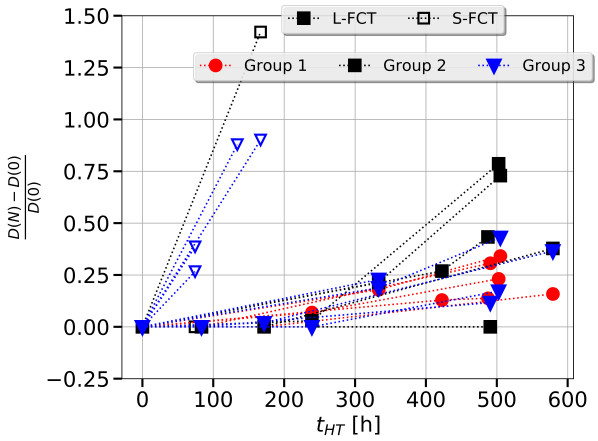

(c) S- and L-FCT function of t_{HT}

Figure 6: Evolution of delamination with thermal cycling for a laser shock achieved in the as-processed condition. (a) corresponds to a global group analysis for L-FCT condition and in (b) and (c) dashed lines connect measurement achieved for each specimen at different number of cycles corresponding to Table 1 for both S- and L-FCT

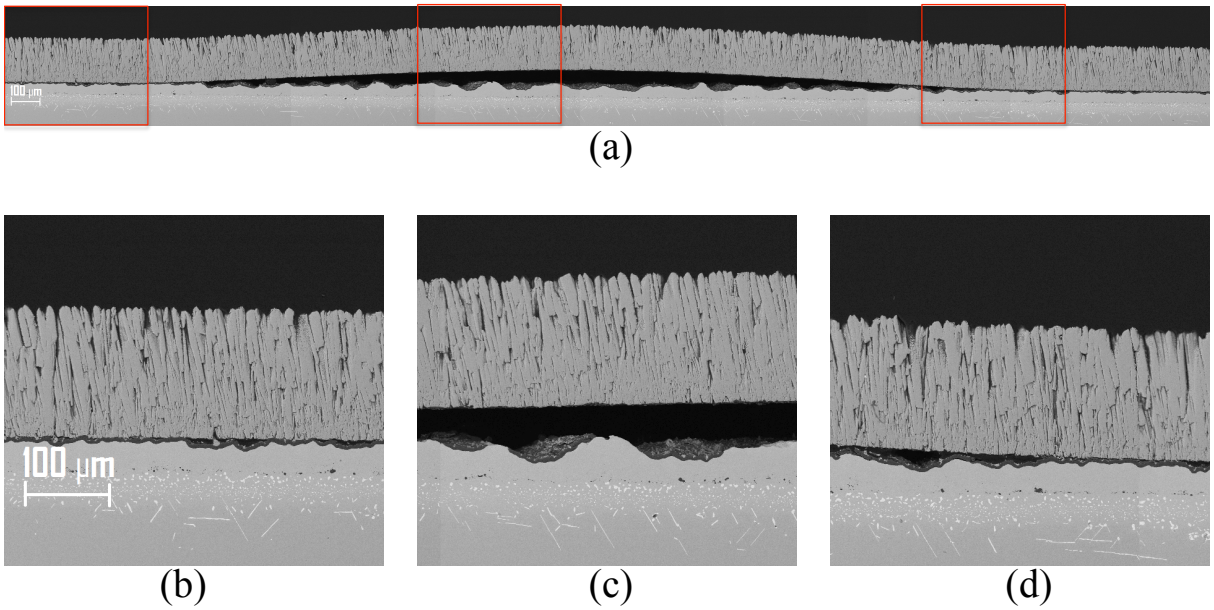

Figure 7: Cross-sectioning of a laser shock achieved in the as-processed condition after 603 cycles with L-FCT condition.

by the presence of cracks. This point should probably explains that after 400 cycles with single laser shock experiment for L-FCT, see Figure 5(a), the experiment yields to a complex evolution of debonding. This is the reason why, it is preferable to address evolution of interfacial strength by LASAT-2D curves instead of single shock method [26]. But, this method prevents from addressing rich database for a limited quantity of samples, because each LASAT-2D curve needs a large size and/or number of coupons.

One of the major result of the present study consists in the robust characterization of a steady-state debonding at the TC/TGO interface consecutively to a laser shock introduced in the as-processed condition. The monotonic evolution of incremental debonding increase appears as a master curves for S- and L-FCT. To confirm these trends, isolating each group (see colors and symbols in figure 6) highlights the difference in behavior from group to group. However, the evolution plot as a function of number of cycles yields a very low scatter of debonding evolution for the whole set of tested specimens as compared to initial scatter.

For the time being it remains unclear why this evolution takes place, we will further elaborate this analysis by comparing with already known results on similar EB-PVD system.

4.2. Comparison with damage measured by cross-sectioning

The TBC system used in this study was also investigated in previous works. To observe damage evolution with thermal cycling, systematic cross-sectionning was achieved [19] and completed by Xray computed laminography[1] to determine if cross-sectioning has impacted

[1]Xray computed laminography is similar to Xray computed tomography but uses a different incidence angle between the beam and the specimen; thus it is possible to analyze specimens with small thickness but

or not the interfacial damage [28]. The consistency of the Xray non destructive testing measurement with observed interfacial cracking validates cross-sectioning measurement method. In other words, the preparation of cross-section does not modify the interfacial cracks by significantly increase of their length or opening. Cross-sectioning observation achieved for the thermal cycling condition referred as S-FCT are reported in Figure 8. During thermal cycling, oxide thickening is obvious together with an increase of local debonding associated to TC/TGO cracks, damage within the oxide thickness, Figure 8(b) or local failure of TC for corn-like defects, Figure 8(c) and (d), and final rumpling. Measuring the length of crack and damaged oxide, Soulignac has proposed to evaluate the ratio in length of interfacial cracking, L_{debond}, to the total length of the observed cross-section, L_{total}, as a damage parameter d_{CS}, eq. 1:

$$d_{CS}(N) = \frac{L_{debond}(N)}{L_{total}} \tag{1}$$

This value of interfacial damage evolution can be evaluated as a function of the number of thermal cycles, Figure 9.

On the other hand, the observation of a steady-state delamination of the debonded area induced by LASAT in the as-received condition can also be regarded as a progressive interfacial damage, referred as d_{LASAT}. The failure of S-FCT and L-FCT were determined in the present study as the spallation of more than 20% of the disk area. This way, an interfacial damage parameter is constrained so that $d_{LASAT}(N_s)$ reaches a value of 1 when the debonded area, defined by the equivalent diameter $D(N_s)$, is equal to 20% of the coupon surface. It comes down to the assumption of a complete damage of the TC/TGO interface when the equivalent debonded diameter reaches $D(N_s)$. Finally, d_{LASAT} is defined as a function of the number of cycles N from measurement of debonded diameter $D(N)$ following:

$$d_{LASAT}(N) = \frac{D(N) - \overline{D(0)}}{D(N_s) - \overline{D(0)}} \tag{2}$$

where $\overline{D(0)}$ corresponds to the mean value of initial debonded area induced by LASAT in the as-processed condition. For S-FCT, damage measured by LASAT analysis d_{LASAT} is fully consistent with damage measured from cross-sectionning, d_{CS}, Figure 9. Moreover, the measured d_{LASAT} for L-FCT is again consistent with the whole set of measured interfacial damage as a function of the number of cycles. Of course, the sensitivity of LASAT questions the comparison of two different batches of specimens. Nevertheless, the consistency of observed damage evolution gives confidence in the robustness of the analysis.

Since damage evolution is, for the tested conditions, a direct function of the number of cycles, we can claim that interfacial damage mechanisms under thermal cycling could be directly seen as a fatigue damage process as already observed for APS coating [3, 21].

large in-plane dimensions

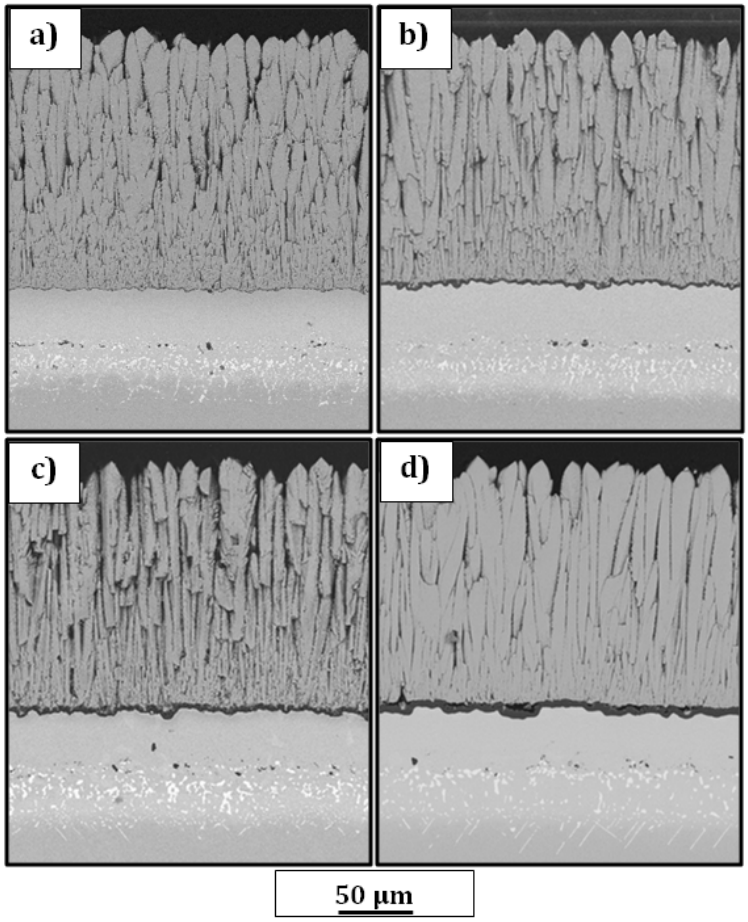

Figure 8: Evolution of microstructure observed by cross-section with thermal cycling without LASAT, in (a) as-processed condition and after (b) 384, (c) 1200 and (d) 2000 S-FCT cycles; from [32].

4.3. Major outcomes

The proposed methodology consists in the characterization of progressive interfacial debonding from a debonded area induced by LASAT. The LASAT is straightforward to know precisely where observation should be performed along thermal cycling. A major gain is that no-edge effect artifacts the evolution of debonding, which is a well known critical aspect of disk-shape coupons. Besides, the measurement by infra-red thermography is an easy method to monitor progressive debonding during test interruptions if the location of defect and the size of defect is large enough to improve the noise to signal ratio. This methodology is straightforward for global damage monitoring in TBC systems, because it has appeared to gain both in easiness of use and robustness. Finally, this method allows a very rapid screening of TC adhesion properties, being of high interest for optimal design of TBCs.

However, the use of a single shock condition at different number of cycles has led to more mitigated results, because of the observed scatter in debonding evolution. The chosen level of laser power density might be too high when samples have been aged as discussed above. A possible alternative is to process with smaller energy or more focused laser shock.

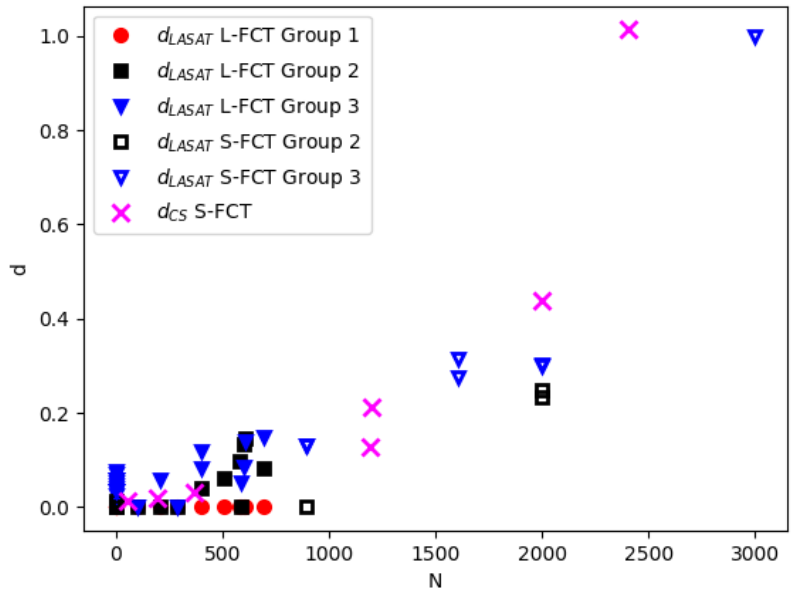

Figure 9: Comparison of damage analysis from cross-sectioning, d_{CS} corresponding to eq. 1 (experimental results from [19, 28]) and laser shock, d_{LASAT} corresponding to eq. 2 (experimental results from this study).

This methodology will be systematically applied in a near future on more complex loading conditions to propose a robust modeling of interfacial damage governing life to spallation of TBCs.

5. Conclusions

This study has enabled to carry out some new findings based on the systematic combination of LASAT and furnace thermal cycling tests. Two different tracks have been investigated. The first one consists in applying a single laser shock with a constant set-up and for different aging, which has led to a large scatter in debonding. The second one consists in monitoring interfacial cracking along thermal cycles from an artificial debonded area achieved in the as-processed condition. This second result was seen to be very promising.

About methodology, the use of infra-red thermography coupled with initial interfacial debonding processed by LASAT has enabled to characterize precisely the interfacial debonding under thermal cycling condition. Main experimental results are for thermal cycling, short dwell time has been confirmed to be more damaging than long dwell time at maximum temperature when comparison is achieved with respect to the cumulated time spent at the maximum temperature. Besides, for the tested conditions, the thermal cycling induces a progressive damage function of the number of cycles. A major finding of this work, that is deduced from the developed methodology, consists in the exhibition of a "fatigue-like" dam-

age derived from the steady-state delamination of the as-processed debonded area, evolution shown to be consistent with interfacial damage observed on cross-section.

Acknowledgement

Part of this work was carried out within the Chair CRISTAL supported by Safran Group and headed by Prof Georges Cailletaud who is deeply acknowledge for his trust. Authors thanks Guillaume Cottin and Lara Mahfouz (Mines ParisTech) and Dana Cosson (Safran Tech) to have performed cross-sectioning and thermal cycling experiments respectively. Sylvain Gailliegue (Mines ParisTech) is also acknowledge for his continuous help in high temperature testing. Alexandre Cottin (Mines ParisTech) is acknowledge for his support in LASAT testing.

References

References

[1] MH Vidal-Setif, N Chellah, C Rio, C Sanchez, and O Lavigne. Calcium–magnesium–alumino–silicate (CMAS) degradation of EB-PVD thermal barrier coatings: Characterization of CMAS damage on ex-service high pressure blade tbcs. *Surface and Coatings Technology*, 208:39–45, 2012.

[2] Daniel E Mack, Tanja Wobst, Maria Ophelia D Jarligo, Doris Sebold, and Robert Vaßen. Lifetime and failure modes of plasma sprayed thermal barrier coatings in thermal gradient rig tests with simultaneous CMAS injection. *Surface and Coatings Technology*, 324:36–47, 2017.

[3] D. Naumenko, V. Shemet, L. Singheiser, and W.-J. Quadakkers. Failure mechanisms of thermal barrier coatings on MCrAlY-type bondcoats associated with the formation of the thermally grown oxide. *Journal of Materials Science*, 44(7):1687–1703, Apr 2009.

[4] NM Yanar, M Helminiak, GH Meier, and FS Pettit. Comparison of the failures during cyclic oxidation of yttria-stabilized (7 to 8 weight percent) zirconia thermal barrier coatings fabricated via electron beam physical vapor deposition and air plasma spray. *Metallurgical and Materials Transactions A*, 42(4):905–921, 2011.

[5] M Gell, L Xie, X Ma, E H Jordan, and N P Padture. Highly durable thermal barrier coatings made by the solution precursor plasma spray process. *Surface and Coatings Technology*, 177:97–102, 2004.

[6] BG Ravi, S Sampath, R Gambino, JB Parise, and PS Devi. Plasma spray synthesis from precursors: Progress, issues, and considerations. *Journal of thermal spray technology*, 15(4):701–707, 2006.

[7] R.A. Miller. Oxidation-based model for thermal barrier coating life. *Journal of the American Ceramic Society*, 67(8):517 – 521, 1984.

[8] R. A. Miller. Life modeling of thermal barrier coatings for aircraft gas turbine engines. *Journal of Engineering for Gas Turbines and Power*, 111(2):301–305, 04 1989.

[9] C. Courcier, V. Maurel, L. Remy, S. Quilici, I. Rouzou, and A. Phelippeau. Interfacial damage based life model for EB-PVD thermal barrier coating. *Surface and Coatings Technology*, 205(13-14):3763 – 3773, 2011.

[10] G.C. Chang, W. Phucharoen, and R.A. Miller. Finite element thermal stress solutions for thermal barrier coatings. *Surface and Coatings Technology*, 32(1):307 – 325, 1987.

[11] E.P. Busso, L. Wright, H.E. Evans, L.N. McCartney, S.R.J. Saunders, S. Osgerby, and J. Nunn. A physics-based life prediction methodology for thermal barrier coating systems. *Acta Materialia*, 55(5):1491 – 1503, 2007.

[12] V. Maurel, E.P. Busso, J. Frachon, J. Besson, and F. N'Guyen. A methodology to model the complex morphology of rough interfaces. *International Journal of Solids and Structures*, 51(19):3293 – 3302, 2014.

[13] D.S. Balint, T. Xu, J.W. Hutchinson, and A.G. Evans. Influence of bond coat thickness on the cyclic rumpling of thermally grown oxides. *Acta Materialia*, 54(7):1815 – 1820, 2006.

[14] J-R Vaunois, J-M Dorvaux, P Kanoute, and J-L Chaboche. A new version of a rumpling predictive model in thermal barrier coatings. *European Journal of Mechanics - A/Solids*, 42:402 – 421, 2013.

[15] V. Maurel, P. de Bodman, and L. Remy. Influence of substrate strain anisotropy in TBC system failure. *Surface and Coatings Technology*, 206(7):1634 – 1639, 2011.

[16] P. Y. Thery, M. Poulain, M. Dupeux, and M. Braccini. Spallation of two thermal barrier coating systems: experimental study of adhesion and energetic approach to lifetime during cyclic oxidation. *Journal of Materials Science*, 44(7):1726–1733, 2009.

[17] J-R Vaunois, M Poulain, P Kanoute, and J-L Chaboche. Development of bending tests for near shear mode interfacial toughness measurement of EB-PVD thermal barrier coatings. *Engineering Fracture Mechanics*, 171:110 – 134, 2017.

[18] O. Trunova, T. Beck, R. Herzog, R.W. Steinbrech, and L. Singheiser. Damage mechanisms and lifetime behavior of plasma sprayed thermal barrier coating systems for gas turbines–part i: Experiments. *Surface and Coatings Technology*, 202(20):5027 – 5032, 2008.

[19] R. Soulignac, V. Maurel, L. Remy, and A. Koster. Cohesive zone modelling of thermal barrier coatings interfacial properties based on three-dimensional observations and mechanical testing. *Surf. Coat. Technol.*, 237(0):95 – 104, 2013.

[20] T Strangman, D Raybould, A Jameel, and W Baker. Damage mechanisms, life prediction, and development of EB-PVD thermal barrier coatings for turbine airfoils. *Surface and Coatings Technology*, 202(4-7):658–664, 2007.

[21] K P Jonnalagadda, R Eriksson, X-H Li, and R L Peng. Fatigue life prediction of thermal barrier coatings using a simplified crack growth model. *Journal of the European Ceramic Society*, 39(5):1869 – 1876, 2019.

[22] N. Yanar, F. Pettit, and G. Meier. Failure characteristics during cyclic oxidation of yttria stabilized zirconia thermal barrier coatings deposited via electron beam physical vapor deposition on platinum aluminide and on NiCoCrAlY bond coats with processing modifications for improved performances. *Metallurgical and Materials Transactions A*, 37(5):1563–1580, 2006.

[23] V. Guipont, M. Jeandin, S. Bansard, K.-A. Khor, M. Nivard, L. Berthe, J.-P. Cuq-Lelandais, and M. Boustie. Bond strength determination of hydroxyapatite coatings on Ti-6Al-4V substrates using the laser shock adhesion test (lasat). *Journal of Biomedical Materials Research Part A*, 95(4):1096–1104, 2010.

[24] G. Bégué, G. Fabre, V. Guipont, M. Jeandin, P. Bilhe, J.-Y. Guedou, and F. Lepoutre. Laser shock adhesion test (LASAT) of EB-PVD TBCs: Towards an industrial application. *Surface and Coatings Technology*, 237:305–312, 2013.

[25] G. Fabre. *Influence des propriétés optiques et de l'endommagement de barrières thermiques EB-PVD pour la mesure d'adhérence par choc laser LASAT-2D (in French)*. PhD thesis, Mines ParisTech, 2013.

[26] V Guipont, G Begue, G Fabre, and V Maurel. Buckling and interface strength analyses of EB-PVD TBC combining laser shock adhesion test (LASAT) to thermal cycling. *Surf. Coat. Technol.*, under edition (special issue 46th ICMCTF), 2019. *https://doi.org/10.1016/j.surfcoat.2019.124938*.

[27] V.K. Tolpygo and D.R. Clarke. Surface rumpling of a (Ni,Pt)Al bond coat induced by cyclic oxidation. *Acta Mater.*, 48:3283–3293, 2000.

[28] V. Maurel, R. Soulignac, L. Helfen, T.F. Morgeneyer, A. Koster, and L. Remy. Three-dimensional damage evolution measurement in EB-PVD TBC using synchrotron laminography. *Oxidat. of Metals*, 79(3-4, SI):313–323, 2013.

[29] M Schweda, T Beck, M Offermann, and L Singheiser. Thermographic analysis and modelling of the delamination crack growth in a thermal barrier coating on FeCr alloy substrate. *Surface and Coatings Technology*, 217:124–128, February 2013.

[30] H Sapardanis, V Maurel, A Köster, S Duvinage, François Borit, and Vincent Guipont. Influence of macroscopic shear loading on the growth of an interfacial crack initiated from a ceramic blister processed by laser shock. *Surface and Coatings Technology*, 291:430–443, 2016.

[31] M Gell, K Vaidyanathan, B Barber, E Jordan, and J Cheng. Mechanism of spallation in platinum aluminide/electron beam physical vapor-deposited thermal barrier coatings. *Metallurgical and Materials Transactions A*, 30:427–435, 1999.

[32] R Soulignac. *Prévision de la durée de vie à l'écaillage des barrières thermiques (in French)*. PhD thesis, Mines ParisTech, 2014.